In silico virtual screening of *Citrus limetta* peel phytocompounds to combat skin cancer targets: Molecular docking and molecular dynamics simulation

Mansi Sharma[1], Rachana R[*]

[1]Jaypee Institute of Information Technology, Sector-62, Noida-201309, U.P., India
Email: mansish41997@gmail.com
*Jaypee Institute of Information Technology, Sector-62, Noida-201309, U.P., India
*Corresponding Email: rachana.dr@iitbombay.org

Abstract

Skin cancer is a persistent global health issue characterized by the dysregulation of critical signalling pathways. MEK1, CDK4, and IL1 have emerged as key therapeutic targets due to their roles in MAPK, CDK4, and IL1 signalling pathways. Although several existing therapies and synthetic inhibitors are available to target these proteins, their clinical use is often associated with adverse effects, highlighting the need for safer alternatives such as phytocompounds. In this study, 15 compounds identified from *Citrus limetta* peel extract were virtually screened against MEK1, CDK4, and IL1, using molecular docking and molecular dynamics (MD) simulation approaches. Pharmacological properties were assessed through ADMET analysis using online prediction tools. Binding affinities were evaluated and compared to the standard inhibitors, revealing that ellagic acid, hesperidin, and quercetin exhibited more favorable binding energies towards MEK1 (−10.5 kcal/mol), CDK4 (−8.8 kcal/mol), and IL1 (−7.6 kcal/mol), respectively. Further MD simulation was performed to examine the structural stability of the complexes, demonstrating stable interactions for ellagic acid-MEK1 and IL1-quercetin complexes, whereas hesperidin-CDK4 showed minor conformational changes towards the end of the simulations. The MMGBSA approach was performed to estimate binding free energies, which validated the docking results. ADMET prediction suggested acceptable drug-like properties with no significant toxicity for most compounds. Based on this study, ellagic acid, hesperidin, and quercetin show promising potential as natural alternatives to synthetic inhibitors commonly used in skin cancer treatment, effectively targeting MEK1, CDK4, and IL1. However, to confirm the therapeutic potential, further *in vivo* and *in vitro* study is needed.

Keywords: Skin Cancer; Target proteins; *Citrus limetta*; Phytocompounds; ADME-T; Molecular docking simulations

1. Introduction

Skin cancer is one of the most commonly occurring cancers, distinguished by the extensive and uncontrolled growth of abnormal skin cells. The primary cause of this cancer is DNA damage induced by ultraviolet (UV) radiation from the sun (Chauhan 2018). Alterations in metabolic pathways are common in cancers, leading to abnormal cell growth, disruptions in the cell cycle, apoptosis, and loss of genomic stability (Sever and Brugge 2015). More than 80% of the cellular pathways involved in cancer development are regulated by protein kinases, which control phosphorylation-dephosphorylation processes (Yousuf et al. 2020). Researchers have shown that the overexpression or dysregulation of kinases such as Mitogen activated protein kinase kinase 1 (MEK1) and Cyclin-dependent kinase 4 (CDK4), along with proteins like Interleukin-1 (IL1), have been linked to skin cancer through activation of downstream signaling pathways that regulate cell proliferation, differentiation, survival, invasion, and tumor progression (Grimaldi et al. 2017; Hamilton and Infante 2016; Garlanda and Mantovani 2021).

MEK1 is a key kinase in regulating the MAPK signaling pathway, which is activated when growth factors bind to receptor tyrosine kinases (RTKs), leading to sequential activation of RAS, RAF kinases, and MEK1. Activated MEK1 then phosphorylates extracellular signal-regulated kinases (ERK1 and ERK2), leading to changes in gene expression that drive cellular responses (Bahar et al. 2023). Dysregulation of the CDK4 pathway is also common in melanoma (Garutti et al. 2021). Overexpression of CDK4 drives the cell cycle transition from the G1 to S phase. CDK4 forms complexes with D-type cyclins and phosphorylates retinoblastoma (RB), releasing E2F transcription factors to drive DNA replication and accelerate the cell cycle (Guo et al. 2020). Dysregulation can occur through overexpression of cyclin D, loss of INK4 inhibitors, RB mutations, or amplification of CDK4. INK4 inhibitors such as $p16^{INK4a}$ control CDK4 activity by

preventing CDK4-Cyclin D binding and halting the cell cycle (Hamilton and Infante 2016). Targeting CDK4 with inhibitors can efficiently stop cell proliferation or cause apoptosis through RB-independent and dependent pathways (Qi and Ouyang 2022). IL-1 is a pro-inflammatory cytokine that induces skin inflammation and hyperproliferation. Overexpression of IL-1α and IL-1β drives inflammation in skin cancer, leading to tumor progression (Bou-Dargham et al. 2017). These findings highlight the potential of targeting MEK1, CDK4, and IL1 for skin cancer therapy.

Several targeted therapies, including FDA-approved inhibitors, are currently available for the treatment of skin cancer. MEK inhibitors such as Cobimetinib, Binimetinib, and Trametinib are currently used in cancer therapy. Cobimetinib, approved in 2015, is a highly selective inhibitor effective against $BRAF^{V600E/K}$-mutated melanoma by suppressing MEK–ERK signaling and tumor cell proliferation (Cheng & Tian 2017; Unsworth et al. 2019). CDK4 inhibitors such as Palbociclib, Ribociclib, and Abemaciclib effectively suppress cell cycle progression (Wander et al. 2022). Abemaciclib, a 3rd generation oral CDK4 inhibitor, selectively binds to the ATP-binding site of the inactive kinase, thereby blocking RB hyperphosphorylation and halting the cell cycle (Garutti et al. 2021). IL-1 inhibitors, such as Anakinra, Rilonacept, and Canakinumab, are approved for clinical use, with Anakinra serving as a recombinant form of the IL-1 receptor antagonist (IL1-RA), which is naturally produced in humans (Malcova et al. 2021). Despite their efficacy, synthetic drugs are often limited by adverse effects and lack of selectivity, which has increased the demand for therapies based on natural compounds derived from plant products that are selectively cytotoxic to cancer cells.

Various plant extracts derived from roots, leaves, fruits, and peels, along with their phytocompounds, have shown potential as effective anti-cancer agents (Chinembiri et al. 2014). *C. limetta* (Mosambi) is a widely consumed fruit, and its peel, constituting 8–10% of the fruit's weight, is rich in bioactive compounds like ascorbic acid, phenols (e.g., rutin), flavonoids (hesperidin, quercetin), carotenoids, and essential oils (Maurya et al. 2018; Buyukkurt et al. 2019; Khan et al. 2016).

Therefore, this *in silico* study was designed to screen selected phytocompounds based on their pharmacokinetic and toxicity profiles using ADMET analysis. The bioactive compounds from *C. limetta* were further validated using molecular docking analysis against MEK1, CDK4, and IL1 to assess their binding affinities. The docking outcomes were further validated through MD simulations to examine the structural stability of the protein ligand complex. For comparative evaluation, the docking performance of the phytocompounds was analyzed against standard inhibitors such as cobimetinib, abemaciclib, and anakinra corresponding to MEK1, CDK4, and IL1 respectively.

2. Materials and methods

2.1 Selection and preparation of protein

MEK1, CDK4, and IL1 crystal structures were obtained from the Protein Data Bank (PDB) in PDB format (available at www.rcsb.org/), as illustrated in Figure 1. The preparation of these proteins involved the elimination of water molecules, the addition of non-polar hydrogens, and the assigning of Kollmann charges, followed by saving the files in PDBQT format. These steps were carried out using AutoDock Vina 1.5.7, integrated with PMV (Python Molecular Viewer) (Lolok et al., 2022).

The CASTp 3.0 was used to verify the functional domains and active binding amino acid residues of each protein. The grid settings were adjusted based on the visualization of the involved amino acids (Kaloni et al., 2020). For protein 3W8Q, the grid center coordinates are (x: 25.192, y: 8.945, z: 11.490 Å) with grid dimensions of (x: 70, y: 64, z: 70). For protein 3G33, the grid center coordinates are (x: 22.900, y: 24.922, z: 30.515 Å) with dimensions of (x: 74, y: 70, z: 90). For protein 9ILB, the grid center coordinates are (x: −13.906, y: 11.813, z: −1.287 Å) with grid dimensions of (x: 48, y: 44, z: 44).

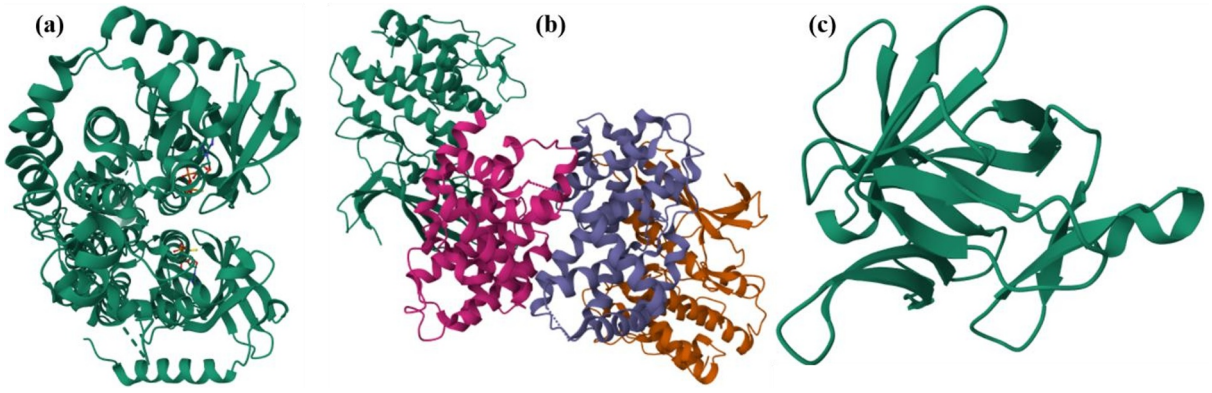

Figure 1. Structures of target proteins (a) MEK1 (PDB ID: 3W8Q), (b) CDK4 (PDB ID: 3G33), (c) IL1 (PDB ID: 9ILB).

2.2 Selection of phytocompounds and standard inhibitor drugs

15 major phytocompounds from *C. limetta* peel, were identified through a literature review, and standard inhibitors of MEK1, CDK4, and IL1 were selected. Specifically, Cobimetinib (PubChem CID: 16222096) is known to inhibit MEK1, Abemaciclib (PubChem CID: 46220502) targets CDK4, and Anakinra (PubChem CID: 90470007) is an inhibitor of IL1 (Figure 2).

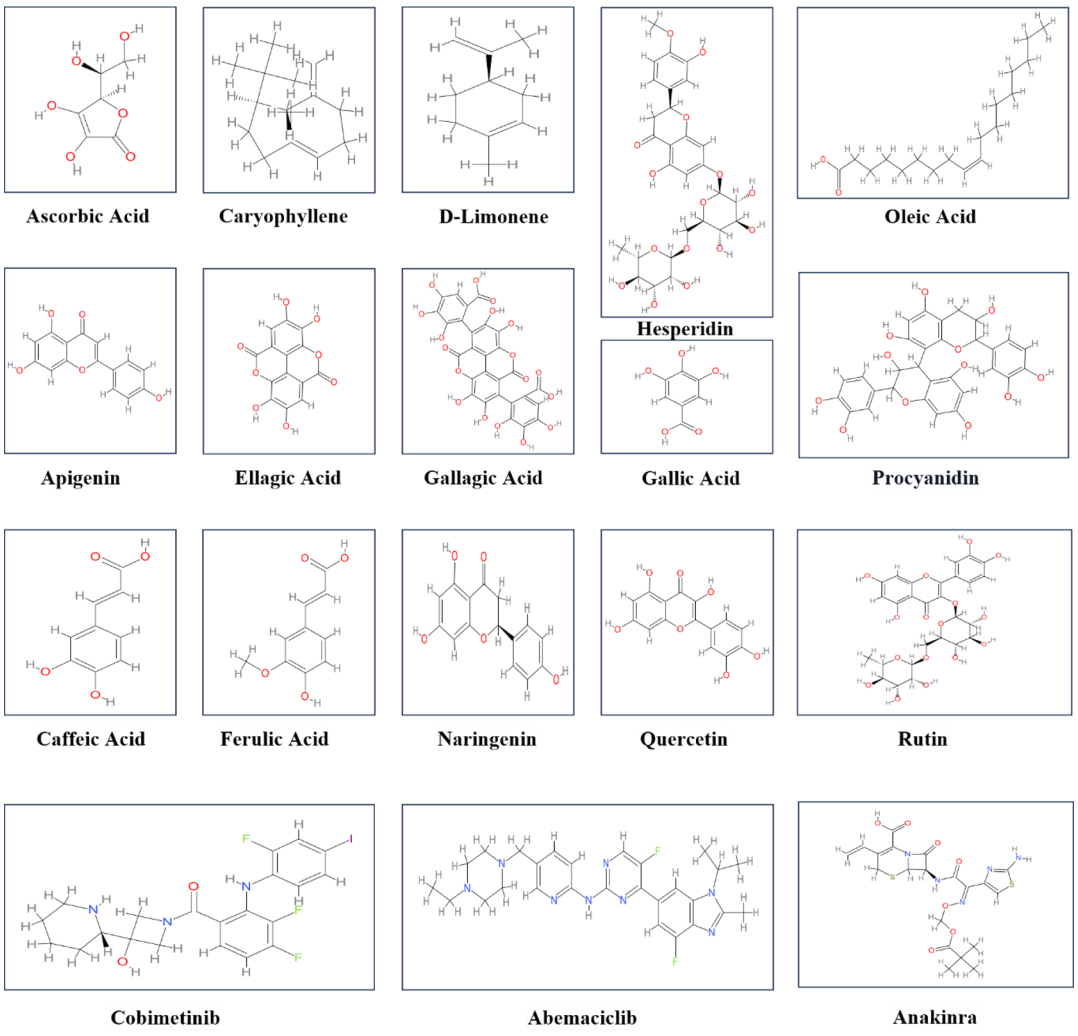

Figure 2. 2D Structures of phytocompounds and drugs used in this study

2.3 Ligand preparation

The chemical structures of the phytocompounds and standard inhibitor drugs were downloaded from the PubChem database (https://pubchem.ncbi.nlm.nih.gov/) in SDF format. The ligands were subsequently converted to PDB format using the Online SMILES Translator and Structure File Generator (https://cactus.nci.nih.gov/translate/) (Thirumalaisamy et al., 2023). Subsequently, AutoDock Vina 1.5.7 parameters were applied to establish proper torsion requirements, followed by conversion to pdbqt format suitable for molecular docking analysis (Mendie & Hemalatha, 2022).

2.4 Prediction of ADME and toxicity by computational analysis

ADMET (Absorption, Distribution, Metabolism, Excretion, and Toxicity) analysis was performed to assess the ligands' absorption, toxicity, drug-likeness, and physicochemical characteristics. The 3D structures of the ligands were saved in SMILES format and uploaded to the SwissADME web server (http://www.swissadme.ch/) for ADME property determination using the Lipinski rule-of-five (Ro5) method (Rolta et al., 2021). According to Lipinski's criteria, a compound is considered drug-like if it satisfies at least three of the following parameters: molecular weight (optimal range <500 g/mol), lipophilicity (log P < 5), hydrogen bond donors (ideally <5), and hydrogen bond acceptors (ideally <10) (Sakshi et al., 2022).

The ProTox-II 2.7 web server was used to assess the toxicity of the ligands (https://tox-new.charite.de/protox_II/). This tool predicts toxicity in several categories, including oral and organ toxicity (e.g., hepatotoxicity), as well as specific toxicological endpoints such as mutagenicity, carcinogenicity, cytotoxicity, and immunotoxicity (Banerjee et al., 2018).

2.5 Molecular docking and visualization

The study was conducted on 15 selected phytocompounds and 3 standard inhibitor drugs targeting MEK1, CDK4, and IL1 using AutoDock Vina 1.5.7. Site-specific docking was performed with specified grid parameters within each protein's active site. The amino acids forming the active site of the protein were identified, and a grid box was established to define the X, Y, and Z coordinates. Binding affinity was then assessed using AutoDock Vina by applying the pdbqt files of the protein and ligand within these defined coordinates. The obtained binding energies were used to compare the relative potency of the phytocompounds with the standard inhibitor drugs. PDB files for each protein-ligand interaction and their binding outcomes were saved for visualization. The 2D binding diagrams and 3D conformations of the ligand-protein interactions were visualized using two AutoDock tools, Biovia Discovery Studio 4.1 and PyMOL 2.5.1 (Sakshi et al., 2022).

2.6 Molecular dynamics (MD) simulation

The study assessed the stability of ligand-protein interactions, focusing on the complexes' structural and functional aspects (Rolta et al., 2021). The analysis was performed on three of the top protein-ligand complexes identified from the docking study. Desmond version 3.6 from the Schrödinger suite (Bowers et al., 2006) was utilized for these simulations, using the Transferable Intermolecular Interaction Potential (TIIP) 3 Points solvent model within an orthorhombic box. The system was neutralized with appropriate counterions, and simulations were carried out using the OPLS_2005 force field parameters. All simulations were carried out at 300 K and maintained at a pressure of 1 atm under the NPT ensemble. A salt concentration (0.15 M) was applied to replicate physiological conditions. Prior to the MD simulations, the model system was allowed to relax. Each simulation was run for 1–100 ns with trajectory snapshots recorded every 50 ps. Root mean square deviation (RMSD) calculations were performed to evaluate the stability of both protein and ligand throughout the simulation period (Noor et al., 2022).

2.7 Molecular mechanics and generalized born surface area (MM-GBSA) calculations

The MM-GBSA method, available in the Prime module, was employed to estimate the binding free energy (ΔGbind) of the docked complexes. This calculation utilized the OPLS 2005 force field, and VSGB solvent model, and included rotamer search techniques. Trajectory frames from the MD simulations were selected at 10 ns intervals after the MD run was completed. The total binding free energy was computed using the following formula:

ΔGbind = Gcomplex − (Gprotein + Gligand)
where ΔGbind = Binding free energy, Gcomplex = Protein-ligand complex free energy, Gprotein = Target protein free energy, and Gligand = Ligand free energy (Kandeel et al., 2023).

3. Results

3.1 Prediction of ADME and toxicity by computational analysis

This study evaluated the pharmacokinetic and physicochemical attributes of natural compounds from *C. limetta* in comparison with standard inhibitor drugs. The phytocompounds and standard inhibitory drugs were analyzed for their ADME properties using an online tool, SWISSADME. Table 1 illustrates that the majority of the phytocompounds satisfied all four criteria of Lipinski's rule. However, hesperidin, gallagic acid, procyanidin, and rutin met at least one criterion, which is still considered acceptable. Among the standard inhibitory drugs, cobimetinib and abemaciclib exhibited one violation each (molecular weight > 500), whereas anakinra showed two violations of molecular weight (optimal range <500 g/mol) and hydrogen bond acceptors (ideally <10).

The ADME prediction parameters detailed in Table 1 indicate that nearly all compounds from *C. limetta* and standard inhibitory drugs may not permeate the blood-brain barrier (BBB), except for D-Limonene, ferulic acid, and cobimetinib. On the other hand, among the compounds studied, only hesperidin, naringenin, and rutin were identified as substrates of P-glycoprotein (P-gp), along with all three standard inhibitor drugs. ADME data further revealed that most of the selected phytocompounds were water-soluble and exhibited significant gastrointestinal (GI) absorption. Specifically, among the standard inhibitor drugs, abemaciclib demonstrated poor water solubility, anakinra exhibited low GI absorption, and cobimetinib displayed good water solubility and high GI absorption. The bioavailability scores for most of the ligands were within acceptable ranges, except for hesperidin, gallagic acid, procyanidin, rutin, and anakinra. The log Kp values of all the ligands were within an acceptable range (–8 to –1 cm/s). These findings suggest the potential of the phytocompounds as they possess drug properties.

Table 1. ADME analysis of the phytocompounds and the standard drugs

Compound	MW (g/mol)	iLogP	H-bond acceptors	H-bond donors	No. of Violations	PGP	GI	BBB	Log Kp (cm/s)	Bioavail. Score	Solubility
Ascorbic Acid	176.12	0.39	6	4	0	No	High	No	-8.54	0.56	Soluble
Caryophyllene	204.3	3.29	0	0	0	No	Low	No	-4.44	0.55	Soluble
D-Limonene	136.23	2.72	0	0	0	No	Low	Yes	-3.89	0.55	Soluble
Hesperidin	610.6	2.60	15	7	3	Yes	Low	No	-10.12	0.17	Soluble
Oleic Acid	282.5	4.27	2	1	0	No	High	No	-2.60	0.85	Mod. soluble
Apigenin	270.24	1.89	5	3	0	No	High	No	-5.80	0.55	Mod. soluble
Ellagic Acid	302.19	0.79	8	4	0	No	High	No	-7.36	0.55	Soluble
Gallagic acid	638.4	-1.03	18	12	3	No	Low	No	-9.29	0.11	Mod. soluble
Gallic Acid	170.12	0.21	5	4	0	No	High	No	-6.84	0.56	Soluble
Procyanidin	578.52	2.05	12	10	3	No	Low	No	-8.15	0.17	Mod. soluble
Caffeic Acid	180.16	0.97	4	3	0	No	High	No	-6.58	0.56	Soluble
Ferulic acid	194.18	1.62	4	2	0	No	High	Yes	-6.41	0.85	Soluble
Naringenin	272.25	1.75	5	3	0	Yes	High	No	-6.17	0.55	Soluble
Quercetin	302.23	1.63	7	5	0	No	High	No	-7.05	0.55	Soluble

Rutin	610.5	1.58	16	10	3	Yes	Low	No	-10.26	0.17	Soluble
Cobimetinib	531.31	3.62	6	3	1	Yes	High	Yes	-6.79	0.55	Mod. soluble
Abemaciclib	506.59	4.16	8	1	1	Yes	High	No	-6.66	0.55	Poorly soluble
Anakinra	509.56	2.39	9	3	1	Yes	Low	No	-8.61	0.11	Mod. soluble

Toxicity prediction

Toxicity and potential adverse effects are critical concerns in the evaluation of therapeutic agents. The results indicated that none of the 15 phytocompounds were predicted to be hepatotoxic. Regarding carcinogenicity, ellagic acid, gallagic acid, gallic acid, and quercetin demonstrated moderate carcinogenic potential, whereas caffeic acid was found to be highly carcinogenic; the remaining compounds were predicted to be non-carcinogenic. With respect to immunotoxicity, caryophyllene exhibited moderate immunotoxicity, whereas hesperidin, procyanidin, ferulic acid, and rutin were classified as strongly immunotoxic. The remaining compounds showed no immunotoxic effects. In terms of mutagenicity and cytotoxicity, all compounds were predicted to be non-mutagenic and non-cytotoxic, except for quercetin and naringenin, which exhibited a moderate probability score for mutagenicity and cytotoxicity, respectively. All the standard inhibitory drugs were non-hepatotoxic, non-carcinogenic, non-immunotoxic, non-mutagenic, and non-cytotoxic (Table 2).

The LD50 values of all selected compounds generally indicate low toxicity. However, Oleic acid, Quercetin, and the standard inhibitor drug Cobimetinib showed comparatively higher toxicity with lower LD50 values. The LD50 values for all compounds ranged from 48 mg/kg (Class II), 315–1172 mg/kg (Class IV), 2500–5000 mg/kg (Class V), 10000–12000 mg/kg (Class VI) (Table 2), suggesting their potential as effective drug candidates with varying degrees of safety profiles.

Table 2. Toxicity of selected phytocompounds and standard inhibitor drugs.

Compound	Hepato-toxicity	Carcino-genicity	Immuno-toxicity	Muta-genicity	Cyto-toxicity	Toxicity Class	LD50
Ascorbic Acid	-	-	-	-	-	5	3367 mg/kg
Caryophyllene	-	-	Moderate	-	-	5	5300 mg/kg
D-Limonene	-	-	-	-	-	5	4400 mg/kg
Hesperidin	-	-	Strong	-	-	6	12000 mg/kg
Oleic Acid	-	-	-	-	-	2	48 mg/kg
Apigenin	-	-	-	-	-	5	2500 mg/kg
Ellagic Acid	-	Moderate	-	-	-	4	2991 mg/kg
Gallagic acid	-	Moderate	-	-	-	4	315 mg/kg
Gallic Acid	-	Moderate	-	-	-	4	2000 mg/kg
Procyanidin	-	-	Strong	-	-	5	2500 mg/kg
Caffeic Acid	-	High	-	-	-	5	2980 mg/kg
Ferulic acid	-	-	Strong	-	-	4	1772 mg/kg
Naringenin	-	-	-	Moderate	Moderate	4	2000 mg/kg
Quercetin	-	Moderate	-	Moderate	-	3	159 mg/kg

Rutin	-	-	Strong	-	-	5	5000 mg/kg
Cobimetinib	-	-	-	-	-	3	300 mg/kg
Abemaciclib	-	-	-	-	-	4	2000 mg/kg
Anakinra	-	-	-	-	-	6	10000 mg/kg

3.2 Molecular docking study

C. limetta peel is rich in phytocompounds, which have been extensively studied worldwide for their potential anti-cancer properties and are believed to possess significant pharmacological activity. Several cancer cell lines, particularly those for the skin, are said to be affected by the antiproliferative and anticancer properties of these phytocompounds. In the current study, 15 phytocompounds present in *C. limetta* peel — ascorbic Acid, caryophyllene, D-Limonene, hesperidin, oleic acid, apigenin, ellagic acid, gallagic acid, gallic acid, procyanidin, caffeic acid, ferulic acid, naringenin, quercetin, and rutin — were investigated via molecular docking against three key proteins involved in skin cancer signaling pathways: MEK1 (PDB ID: 3W8Q), CDK4 (PDB ID: 3G33), and IL1 (PDB ID: 9ILB). Three well-known drug inhibitors, cobimetinib, abemaciclib, and anakinra, of each target protein were employed as references for comparison. The ligands were docked into the binding sites of each target protein (Figure 3), and the binding energies of the resulting complexes were calculated to determine potential therapeutic candidates with high binding affinity for the targets. Lower energy values indicate stronger binding affinity. A detailed analysis of the results is provided below.

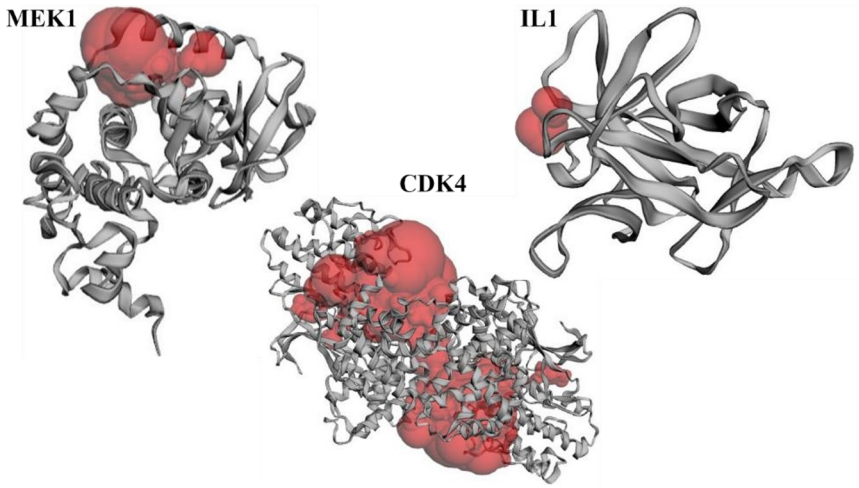

Figure 3. The binding pocket of the target proteins

3.2.1 MEK1

MEK1 serves as a downstream target in the RAS/MAPK signaling pathways, crucial for regulating normal cell proliferation, survival, differentiation, and tumor growth. The molecular docking analysis of the selected phytocompounds and the standard drug inhibitor (Cobimetinib) against MEK1 is described in Table 3. Among the selected compounds, ellagic acid (−10.5 kcal/mol), quercetin (−9.5 kcal/mol), procyanidin (−9.4 kcal/mol), rutin (−9.2 kcal/mol), and apigenin (−9.1 kcal/mol) demonstrated stronger binding affinities compared to cobimetinib (−8.2 kcal/mol). The interaction analysis of the Ellagic acid-MEK1 complex using Discovery Studio (Figure 4, Table 3) revealed the formation of three hydrogen bonds with the residues Met 146, Gly 149, and Gln 153. Additionally, hydrophobic interactions were observed with Leu 74, Val 82, Ala 95, Met 143, Leu 197, and Cys 207, along with van der Waals interactions involving Gly 75, Ala 76, Gly 77, Lys 97, Val 127, Glu 144, His 145, Ser 150, Asp 152, and Ser 194. In contrast, quercetin formed four hydrogen bonds (Leu 74, Ala 76, Met 146, Ser 150) and four hydrophobic interactions (Val 82, Ala 95, Leu 197, Cys 207). From the molecular interactions of docking complexes, procyanidin formed seven hydrogen bond interactions with amino acids Arg 49, Tyr 125, Lys 168, Arg 201, Asp 365, Phe 371, Ala 372, rutin interacted with eight potent hydrogen bond interactions involving amino acids Gln 46, Arg 49, Pro 124, Lys 168, Lys 175, Arg 201, Gly 202, Ile 204, Asp 365 and apigenin formed four hydrogen bond interactions with amino acids Ala 76, Lys 97, His 145, and Ser 150

against MEK1 (Table 3). This suggests that procyanidin and rutin may exhibit an alternative binding mode, possibly interacting with a secondary or allosteric site on MEK1 rather than the canonical active site. According to the docking data, ellagic acid exhibited the strongest affinity against MEK1, whereas oleic acid showed the weakest binding affinity, suggesting that ellagic acid may be a more potent inhibitor of MEK1 compared to the standard drug inhibitor cobimetinib.

Table 3. The predicted binding energy of phytocompounds and standard inhibitor drug against the respective protein targets MEK1.

Source	Ligand	Binding Energy (kcal/mol)	H-bonds	Interacting Amino acids	van der Waals interaction	Hydrophobic interactions
C. limetta peel	Ascorbic Acid	-5.1	1	Gly 202	Gln 46, Arg 49, Pro124, Tyr 125, Ala 171, Glu 205, Lys 205	—
	Caryophyllene	-7.1	0	—	Leu 40, Glu 41, Ser 123, Pro 124,	Leu 42, Tyr 125, Lys 175,
					Gly 176, Thr 178, Glu 182	Tyr 179, Lys 183
	D-Limonene	-6.5	0	—	Lys 97, Met 143 & 146, Gly149	Leu 74, Val 82, Ala 95, His 145, Leu 197, Cys 207
	Hesperidin	-9.0	8	Asp 43, Gln 46, Arg 49, Lys 168, Ala 172, Gly 202, Ile 204, Asp 365	Glu 39, Glu 41, Leu 42, Gln 45, Tyr 125, Ile 171, Lys 175, Glu 203, Ala 366, Glu 367	Pro 124
	Oleic Acid	-4.8	2	Asp 43, Tyr 125	Gln 46, Lys 175, Gly 202, Glu 203, Phe 371	Lys 168, Ile 171, Ala 172, Ile 204
	Apigenin	-9.1	4	Ala 76, Lys 97, His 145, Ser 150	Gly 75, Gly 77, Gly 149, Ser 194, Phe 209, Gly 210	Leu 74, Val 82, Ala 95, Leu 197, Cys 207
	Ellagic Acid	-10.5	3	Met 146, Gly 149, Gln 153	Gly 75, Ala 76, Gly 77, Lys 97, Val 127, Glu 144, His 145, Ser 150, Asp 152, Ser 194	Leu 74, Val 82, Ala 95, Met 143, Leu 197, Cys 207
	Gallagic acid	-7.9	5	Glu 41, Tyr 125, Gly 202, Asp 365, Phe 371	Glu 39, Leu 40, Leu 42, Asp 43, Gln 45, Gln 46, Arg 49, Lys 168, Ile 171, Arg 201, Glu 203, Glu 368, Asp 370, Gly 373	—
	Gallic Acid	-6.5	3	Met 146, Ser 150, Gln 153	Gly 75, Ala 95, Val 127, Glu 144, His 145, Gly 149, Cys 207	Leu 74, Val 82, Leu 197
	Procyanidin	-9.4	7	Arg 49, Tyr 125, Lys 168, Arg 201, Asp 365, Phe 371, Ala 372	Asp 43, Pro 124, Ala 172, Lys 175, Gly 202, Glu 203, Ile 204, Lys 205, Ser 364, Glu 367, Glu 368, Val 369, Gly 373, Asp 370	Gln 46, Ile 171
	Caffeic Acid	-7.2	1	Lys 97	Val 127, His 145, Gly 149, Cys 207, Phe 209	Leu 74, Val 82, Ala 95, Met 143, Leu 197

	Ferulic acid	-6.9	3	Ala 76, Ser 150, Gln 153	Gly 75 & 77, Lys 97, Val 127, Glu 144, His 145, Met 146, Asp 208	Leu 74, Val 82, Ala 95, Met 143, Leu 197, Cys 207
	Naringenin	-8.8	1	Met 146	Gly 75, Ala 76, Gly 77, Met 143, His 145, Gly 149, Ser 150, Ser 194, Asp 208, Phe 209, Gly 210, Val 211	Leu 74, Val 82, Ala 95, Cys 207
	Quercetin	-9.5	4	Leu 74, Ala 76, Met 146, Ser 150	Gly 75 & 77, Asn 78, Lys 97, His 145, Gly 149, Gln 153, Ser 194, Phe 209, Gly 210	Val 82, Ala 95, Leu 197, Cys 207
	Rutin	-9.2	8	Gln 46, Arg 49, Pro 124, Lys 168, Lys 175, Arg 201,	Gln 45, Glu 203, Lys 205, Val 369, Phe 371, Ala 372	Asp 43, Tyr 125, Ile 171, Ala 172
				Gly 202, Ile 204, Asp 365		
Standard drug	Cobimetinib	-8.2	2	Asp 43, Gly 202	Gln 45, Gln 46, Arg 49, Tyr 125, Ala 172, Arg 201, Glu 368, Glu 367, Val 369, Phe 371	Lys 168, Glu 203, Ile 204

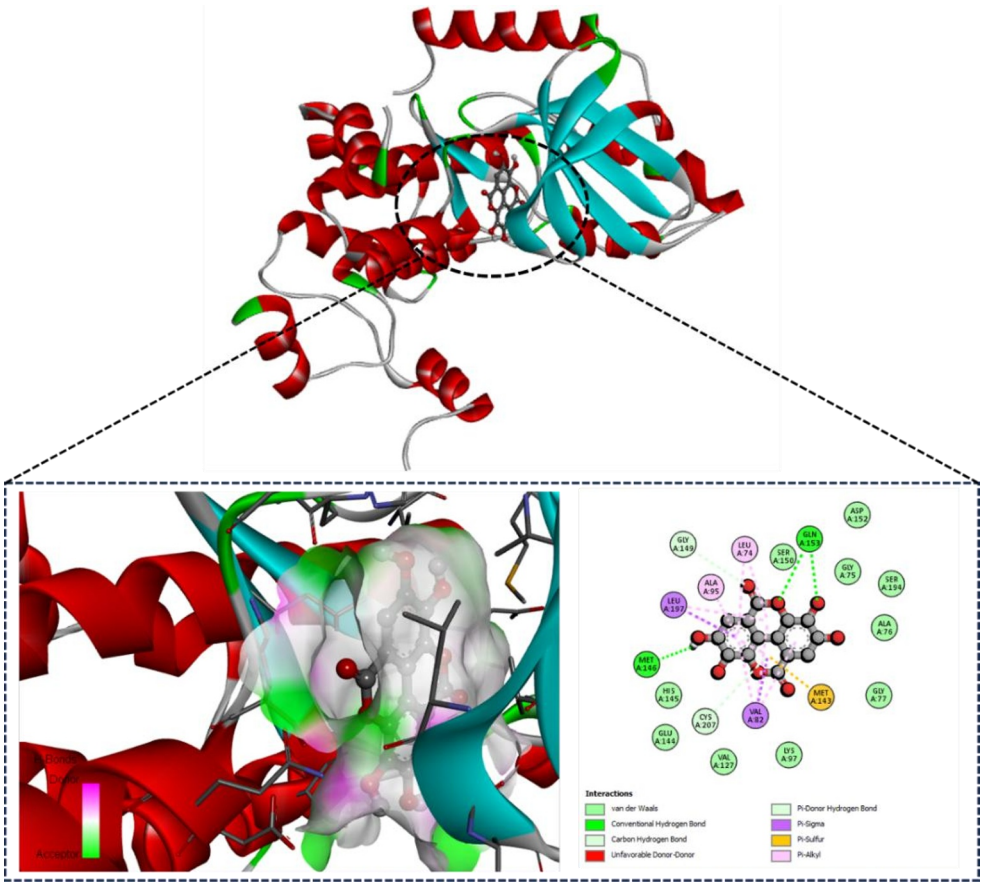

Figure 4. The 3D interaction of Ellagic Acid at MEK1 (3W8Q) binding pocket and 2D visualisation of interaction between Ellagic-MEK1 complex

3.2.2 CDK4

In this study, 15 bioactive compounds from *C. limetta* peel, along with a clinically used CDK4 inhibitor, abemaciclib,

were screened against CDK4, and their binding energies were analyzed (Table 4). Among the selected phytocompounds, hesperidin (−8.8 kcal/mol), quercetin (−8.7 kcal/mol), apigenin (−8.6 kcal/mol), and naringenin (−8.5 kcal/mol) exhibited stronger binding affinities than abemaciclib (−7.8 kcal/mol) (Table 4). Hesperidin binds firmly to the active region of the CDK4, stabilizing the interaction through five conventional hydrogen bonding involved with His 27, Arg 61, Glu 64, Arg 87, and Leu 148 amino acid residues. Additional stabilization was achieved through van der Waals interaction with Arg 5, Tyr 6, Asp 25, Ser 28, Thr 37, Ala 39, Pro 40, Ser 41, Met 75, Asp 76, Ser 90, Leu 91, and hydrophobic interaction with Lys 149 (Table 4, Figure 5). Quercetin interacts with CDK4 active site by forming conventional hydrogen bonds with Val 96, Asp 97, van der Waals interaction with Gly 13, Val 14, Gly 15, Ala 16, Tyr 17, Ala 33, Lys 35, His 95, Gln 98, Asp 99, Asp 140, Glu 144, Asn 145, Asp 158 and hydrophobic interactions with Ile 12, Val 20, Lys 142, Leu 147. The weakest binding affinity was observed between the Oleic Acid-CDK4 complex (−4.5 kcal/mol). Although abemaciclib has a significant binding affinity, it forms only one H-bond with the amino acid His 163. Despite abemaciclib's established role as a CDK4 inhibitor, Hesperidin showed the lowest binding energy and highest binding affinity among the tested phytocompounds, suggesting it may be one of the most effective candidates for targeting CDK4.

Table 4. The predicted binding energy of phytocompounds and standard inhibitor drug against respective protein targets CDK4.

Source	Ligand	Binding Energy (kcal/mol)	H-bonds	Interacting Amino acids	van der Waals interaction	Hydrophobic interactions
C. limetta peel	Ascorbic Acid	-5.1	3	Tyr 17, Ser 36, Gln 168	Gly 18, Thr 19, Lys 35, Val 37, Arg 38, Lys 88, Tyr 165	—
	Caryophyllene	-6.1	0	—	Glu 69, Cys 73, Glu 74, Glu 75, Val 77, Phe 78, Pro 79, Gln 183, Thr 184	Leu 65, Cys 68, Ala 187
	D-Limonene	-7.5	0	—	Gly 224 & 247	Ala 220, Phe 227, Leu 223 & 23, Trp 238, Arg 246, Phe 249
	Hesperidin	-8.8	5	His 27, Arg 61, Glu 64, Arg 87, Leu 148	Arg 5, Tyr 6, Asp 25, Ser 28, Thr 37, Ala 39, Pro 40, Ser 41, Met 75, Asp 76, Ser 90, Leu 91	Lys 149
	Oleic Acid	-4.5	2	Lys 180, Thr 184	Leu 65, Glu 69, Glu 74, Glu 75, Phe 78, Pro 79, Gln 183	Cys 68, Lys 72, Cys 73, Ala 187
	Apigenin	-8.6	1	Gly 15	Gly 13, Val 14, Lys 35, Val 72, Phe 93, Glu 94,	Ile 12, Val 20, Ala 33, Glu

					His 95, Val 96, Asp 99	144, Leu 147, Ala 157
	Ellagic Acid	-8.0	2	Lys 35, Asp 99	Gly 13, Gly 15, Val 72, Phe 93, Glu 94, His 95, Val 96, Asp 97, Gln 98, Asp 158	Ile 12, Val 20, Ala 33, Glu 144, Leu 147
	Gallagic acid	-8.1	5	Tyr 6, Ala 39, Glu 64, Arg 73, Met 75	Arg 5, Asp 25, His 27, Ser 28, His 30, Glu 36, Thr 37, Cys 38, Pro 40, Asp 76, Arg 87, Leu 91, Lys 147, Asn 151	Arg 61
	Gallic Acid	-6.2	3	His 95, Asn 145, Asp 158	Ala 33, Glu 94, Val 96, Asp 99, Glu 144	Ile 12, Val 20, Lys 35, Leu 147, Ala 157
	Procyanidin	-7.8	3	Pro 79, Gln 183, Thr 184	Leu 65, Cys 68, Lys 72, Cys 73, Glu 75, Phe 78, Arg 179	Ala 187
	Caffeic Acid	-6.7	0	—	Leu 187, Ala 220, Gly 224, Leu 232, Trp 238, Pro 245, Arg 246, Gly 247, Ala 248, Phe 249, Pro 250, Arg 252	Leu 223, Phe 227
	Ferulic acid	-6.6	2	Val 96, Glu 144	—	Ile 12, Val 20, Ala 33, Val 72, Phe 93, His 95, Ala 157
	Naringenin	-8.5	2	Val 14, Gly 15	Gly 13, Lys 35, Val 72, Phe 93, Glu 94, His 95, Val 96, Asp 99	Ile 12, Val 20, Ala 33, Glu 144, Leu 147, Ala 157
	Quercetin	-8.7	2	Val 96, Asp 97	Gly 13, Val 14, Gly 15, Ala 16, Tyr 17, Ala 33, Lys 35, His 95, Gln 98, Asp 99, Asp 140, Glu 144, Asn 145, Asp 158	Ile 12, Val 20, Lys 142, Leu 147
	Rutin	-8.2	6	Ala 39, Arg 61, Glu 64, Met 75, Lys 149	Tyr 6, Thr 37, Cys 38, Pro 40, Ser 41, Asp 76, Ser 90, Leu 148	His 27, Arg 73, Arg 87, Leu 91
Standard drug	Abemaciclib	-7.8	1	His 163	Asn 24, Val 27, Met 31, Arg 62, Phe 66, Asn 134, Asp 159, Leu 165, Lys 175	Met 155, Glu 162

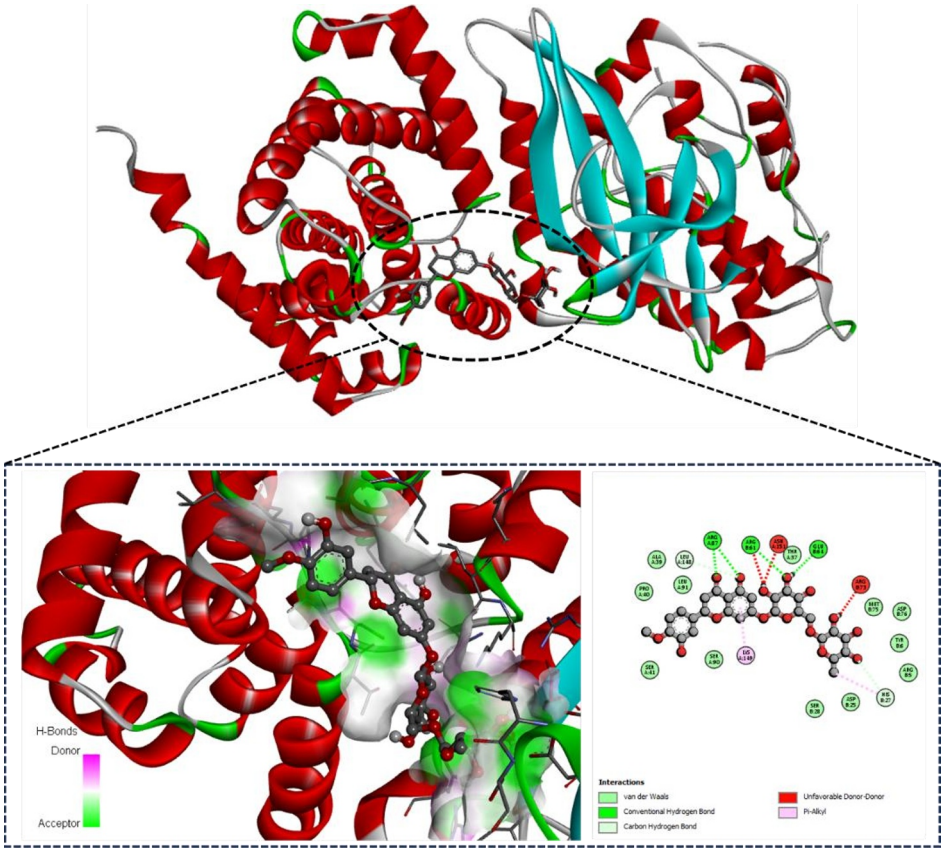

Figure 5. The 3D interaction of Hesperidin at CDK4 (3G33) binding pocket and 2D visualisation of interaction between Hesperidin-CDK4 complex

3.2.3 IL1

IL1, a cytokine, plays a crucial role in cancer development, as the inflammatory response associated with malignancy is regulated by this cytokine. Molecular docking analysis was conducted on 15 selected phytocompounds and the standard inhibitor drug, Anakinra, targeting IL1 (see Table 5). Among the tested phytocompounds, quercetin (−7.6 kcal/mol), hesperidin (−7.5 kcal/mol), rutin (−7.4 kcal/mol), and gallagic acid (−7.4 kcal/mol) demonstrated stronger binding affinities than anakinra (−7.5 kcal/mol) (Table 5). Docking interaction revealed that quercetin interacts with the IL1 active site by forming conventional hydrogen bonds with amino acids Asn 7, Ser 43, Glu 64, Lys 65, Ser 153, van der Waals interaction with Ser 5, Gly 61, Leu 62, Asn 66, Leu 67, and hydrophobic interactions with Lys 63, Pro 91 (Figure 6, Table 5). Similarly, Hesperidin formed hydrogen bonds with Ser 5, Pro 87, Tyr 90, and Ser 153, van der Waals interactions with Ala 1, Val 3, Arg 4, Asn 7, Ser 43, Leu 62, Glu 64, Asn 66, Tyr 68, and Pro 91, and hydrophobic interactions involving Lys 63 and Lys 65. In contrast, the lowest binding affinity was observed for the complexes, the D-Limonene-IL1 and Oleic Acid-IL1 (−4.6 kcal/mol). Anakinra formed seven hydrogen bonds with Val 3, Ser 5, Asn 7, Glu 64, Lys 65, Tyr 68, and Ser 153. Among all the phytocompounds, quercetin exhibited the strongest binding affinity, as indicated by its lowest binding energy.

Table 5. The predicted binding energy of phytocompounds and standard inhibitor drug against the respective protein targets IL1.

Source	Ligand	Binding Energy (kcal/mol)	H-bonds	Interacting Amino acids	van der Waals interaction	Hydrophobic interactions
C. limetta peel	Ascorbic Acid	-5.2	1	Tyr 68	Ser 43, Ser 45, Gly 61, Leu 62, Lys 63, Glu 64, Asn 66, Leu 67, Tyr 90, Pro 91	Lys 65
	Caryophyllene	-5.5	0	—	Gln 39, Val 41, Lys 63, Glu 64	Met 20, Val 40, Leu 62, Lys 65

	D-Limonene	-4.6	0	—	Ser 125, Met 130, Asp 142	Pro 131, Phe 133
	Hesperidin	-7.5	4	Ser 5, Pro 87, Tyr 90, Ser 153	Ala 1, Val 3, Arg 4, Asn 7, Ser 43, Leu 62, Glu 64, Asn 66, Tyr 68, Pro 91	Lys 63, Lys 65
	Oleic Acid	-4.6	2	Ser 152, Ser 153	Asn 7, Gln 38, Gln 39, Val 151	Met 20, Val 40, Val 41, Lys 45, Leu 62, Lys 63
	Apigenin	-7.1	3	Asn 7, Tyr 68, Ser 153	Ser 43, Gly 61, Leu 62, Glu 64, Lys 65, Asn 66, Leu 67, Val 85, Pro 87, Tyr 90, Pro 91	Lys 63
	Ellagic Acid	-7.0	3	Gln 14, Gln 126, Gln 141	Asn 107, Lys 109, Gly 139, Asp 142, Thr 144	Gly 140, Ile 163
	Gallagic acid	-7.4	2	Ser 43, Ser 153	Arg 4, Ser 5, Leu 6, Asn 7, Leu 62, Lys 63, Lys 65, Asn 66, Tyr 68, Pro 87, Tyr 90, Pro 91	Glu 64
	Gallic Acid	-5.2	5	Ser 5, Ser 43, Ser 45, Leu 62, Lys 65	Gly 61, Glu 64, Asn 66, Leu 67, Tyr 68	Pro 91
	Procyanidin	-7.3	4	Asn 7, Ser 43, Lys 65, Ser 153	Pro 2, Val 3, Ser 5, Gly 61, Leu 62, Lys 63, Glu 64, Asn 66, Leu 67, Pro 87, Lys 88, Tyr 90	Tyr 68
	Caffeic Acid	-5.4	5	Ser 13, Gln 14, Gln 126, Gly 139, Thr 144	Glu 111, Gly 140, Asp 142, Ile 143, Lys 138	Asp 145
	Ferulic acid	-5.6	3	Met 20, Gln 38, Lys 63	Val 19, Gln 39, Lys 65	Val 40, Leu 62

	Naringenin	-7.0	3	Lys 65, Tyr 68, Pro 87	Ser 5, Ser 43, Gly 61, Leu 62, Glu 64, Leu 67, Val 85, Tyr 90, Pro 91, Ser 153	Asn 7, Lys 63
	Quercetin	-7.6	5	Asn 7, Ser 43, Glu 64, Lys 65, Ser 153	Ser 5, Gly 61, Leu 62, Asn 66, Leu 67	Lys 63, Pro 91
	Rutin	-7.4	5	Asn 7, Ser 43, Leu 62, Glu 64, Lys 65	Ser 5, Gly 61, Asn 66, Leu 67, Tyr 68, Ser 153	Lys 63, Pro 91
Standard drug	Anakinra	-7.5	7	Val 3, Ser 5, Asn 7, Glu 64, Lys 65, Tyr 68, Ser 153	Ala 1, Arg 4, Ser 43, Gly 61, Leu 62, Lys 63, Asn 66, Leu 67, Pro 87, Tyr 90, Phe 150, Val 151, Ser 152	Leu 6, Pro 91

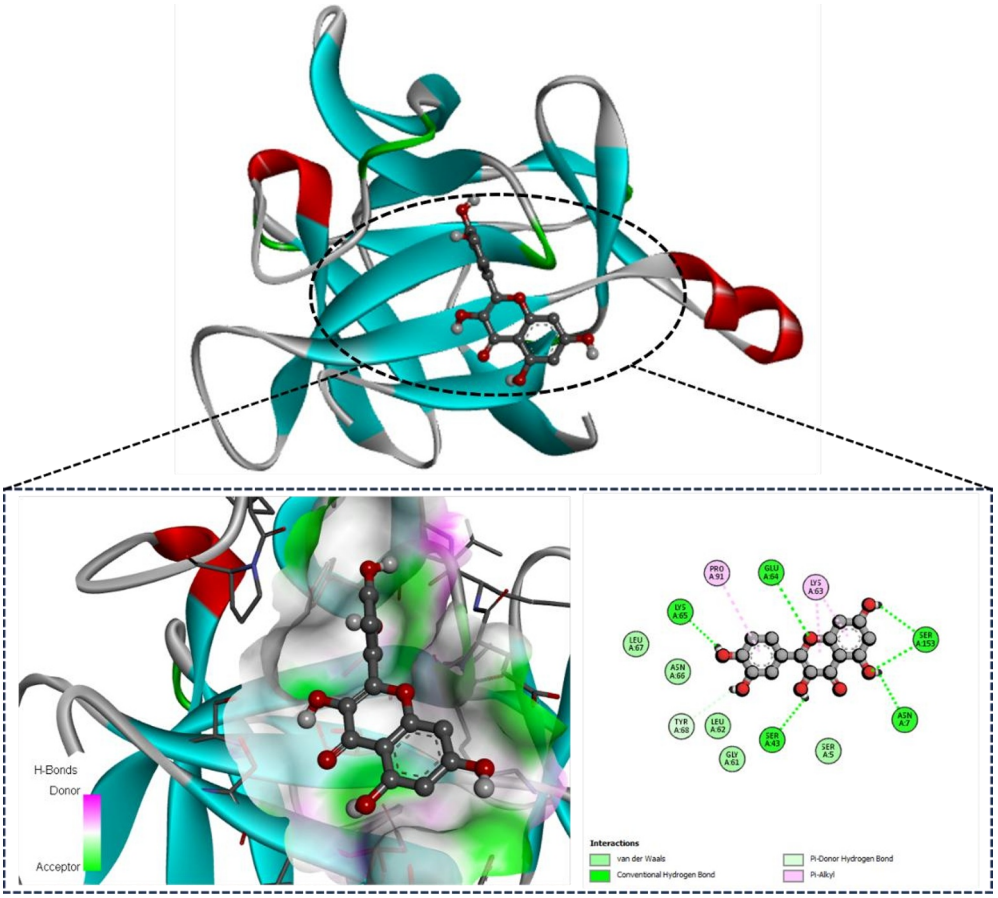

Figure 6. The 3D interaction of Quercetin at IL1 (9ILB) binding pocket and 2D visualisation of interaction between Quercetin-IL1 complex

Among the 15 phytocompounds isolated from *C. limetta* peel, Ellagic acid exhibited a docking score of −10.50 kcal/mol against MEK1, Hesperidin showed a score of −8.8 kcal/mol against CDK4, and Quercetin had a score of −7.6 kcal/mol against IL1. These compounds demonstrated superior potential compared to the standard inhibitors. The promising complexes will be further investigated through MD simulation.

3.3 MD simulation

The best protein-ligand complexes were selected for MD simulation based on the molecular docking results. Three complexes — Ellagic acid-MEK1, Hesperidin-CDK4, and Quercetin-IL1 — were simulated over a 100 ns period, with the results shown in Figures 7, 8, 9, and 10. The plots depict the progression of RMSD for the protein (left Y-axis). RMSD values were calculated by aligning the protein frames to a reference frame's backbone, providing insights into the structural conformation of the protein throughout the simulation. The RMSD is used to evaluate whether the simulation has reached equilibrium, indicated by fluctuations stabilizing around a thermal average structure toward the end of the

simulation. The ligand RMSD (right Y-axis) illustrates the ligand's stability relative to the protein and its binding pocket. The "Lig fit Prot" plot shows the ligand's RMSD after the protein-ligand complex is aligned to the protein backbone, followed by the calculation of the RMSD for the ligand's heavy atoms.

For the Ellagic acid-MEK1 complex over the 100 ns MD simulation, the Cα RMSD of the protein increased during the first 40 ns, reaching around 4.8 Å, indicating conformational adjustment. Thereafter, the protein stabilized between 4.2 and 4.8 Å suggesting structural equilibrium. The ligand RMSD showed fluctuation for the first 40 ns between 1.2–3.2 Å and subsequently gets stabilized around 3.6 Å, indicating stable binding with minor positional variability. Overall, the complex maintained structural stability throughout the simulation (Figure 7(a)).

For the Hesperidin-CDK4 complex, the protein Cα RMSD reached 4.6–5.5 Å within 20 ns, indicating equilibration. A spike occurs around 60 ns, suggesting a conformational change. Thereafter, the protein stabilizes within 5–7 Å, suggesting some structural variability. The ligand exhibited low RMSD values 1.0 to 3.5 Å up to 60 ns, indicating stability within the binding pocket. However, after 60 ns, the ligand's RMSD increased sharply to 14–15 Å. This suggests significant displacement or partial movement from the binding pocket. A longer simulation may be required for the ligand to stabilize, particularly considering its larger molecular size (Figure 7(b)).

For the Quercetin-IL1 complex, the protein RMSD increased to 1.8–2.0 Å, within 10 ns, and stabilized between 1.8–2.4 Å indicating structural stability. The ligand RMSD starts below 0.5 Å during the initial 10 ns and then remains stable within 1.0–2.0 Å indicating strong binding with minor conformational changes. Overall, the complex showed stable interaction throughout the simulation (Figure 7(c)).

(a)

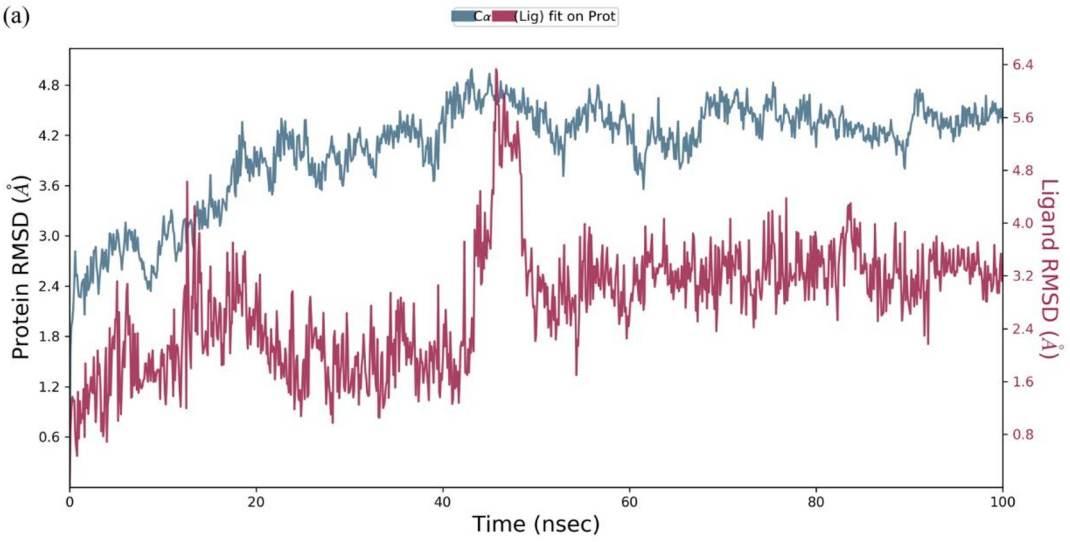

(b)

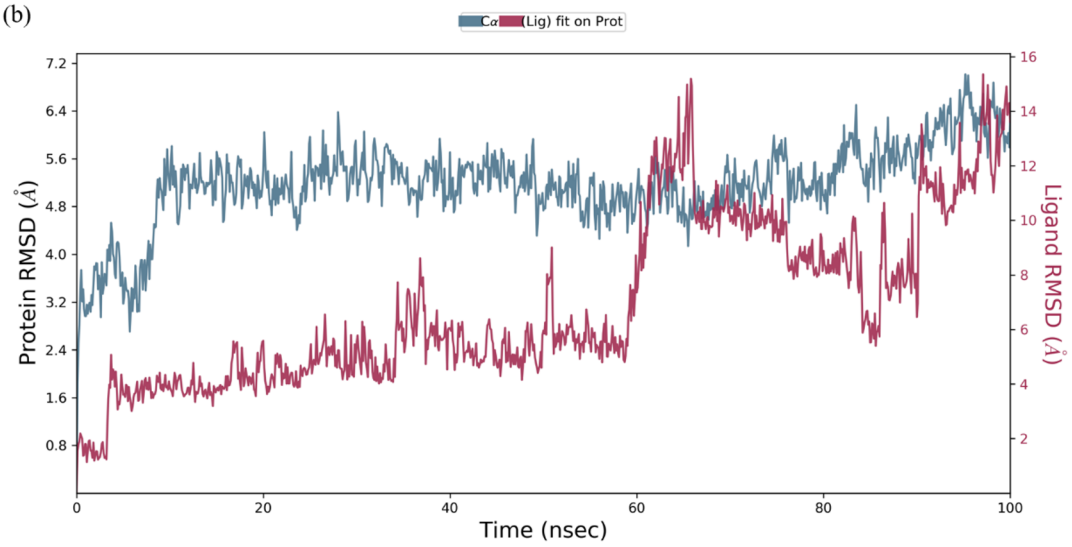

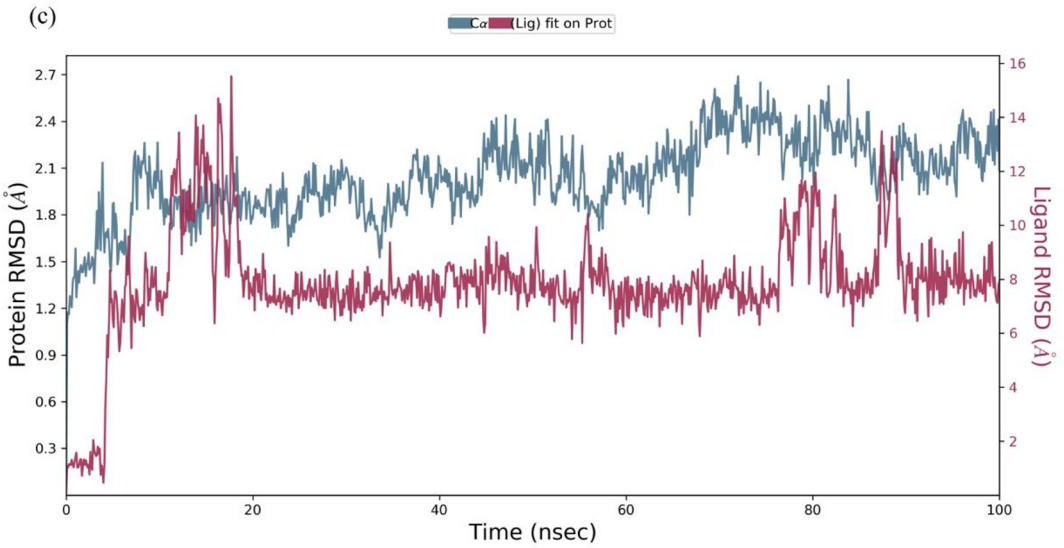

Figure 7. The Graph shows the RMSD measure of the protein-ligand complexes during the entire simulation. The left y-axis depicts the variance in target protein RMSD over time, whereas the right y-axis depicts the variation in ligand RMSD over time. (a) MEK1-Ellagic acid (b) CDK4-Hesperidin (c) IL1-Quercetin

The contact profiles from the MDS study are shown in Figure 8. In the Ellagic acid-MEK1 complex ellagic acid interacted with MEK1 through hydrogen bonding involving residues LEU74, ALA76, ASN98, LYS97, GLU144, MET146, SER150, GLN153, SER194, CYS207, and ASP208. The residues, ASP152, formed water bridges. Notably, MET146 remained in contact for nearly 90% of the simulation time, highlighting its importance in ligand stabilization (Figure 8(a)).

In the CDK4-Hesperidin complex, the ligand interacted with ARG87 and GLU64 by forming hydrogen bonds. These residues maintained significant contact with the ligand for most of the simulation. The other residues involved in the interaction are depicted in Figure 8(b). The compound quercetin interacted with LEU62 and TYR68 by forming strong hydrogen bonds. The residues SER43, LEU62, GLU64, LYS65, ASN66, and LEU67 contributed to the formation of water bridges. Additionally, PRO87 and PRO91 were involved in hydrophobic interactions Figure 8(c).

Across all complexes, a variety of interactions were observed, including hydrophobic interactions, ionic bonds, and water bridge interactions. Furthermore, the protein-ligand interaction timeline graph revealed significant interactions for Ellagic acid-MEK1, Hesperidin-CDK4, and Quercetin-IL1 (Figure 9). These results reveal that Ellagic acid, Hesperidin, and Quercetin may have potential modulatory effects on the respective target proteins.

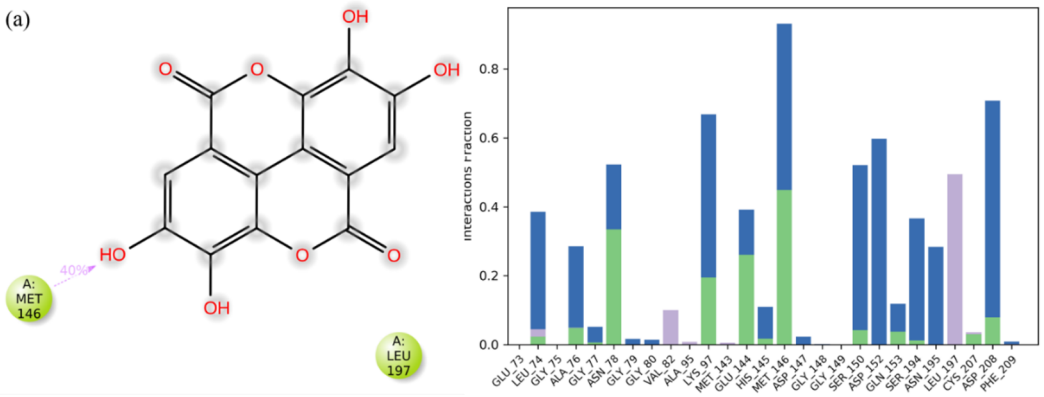

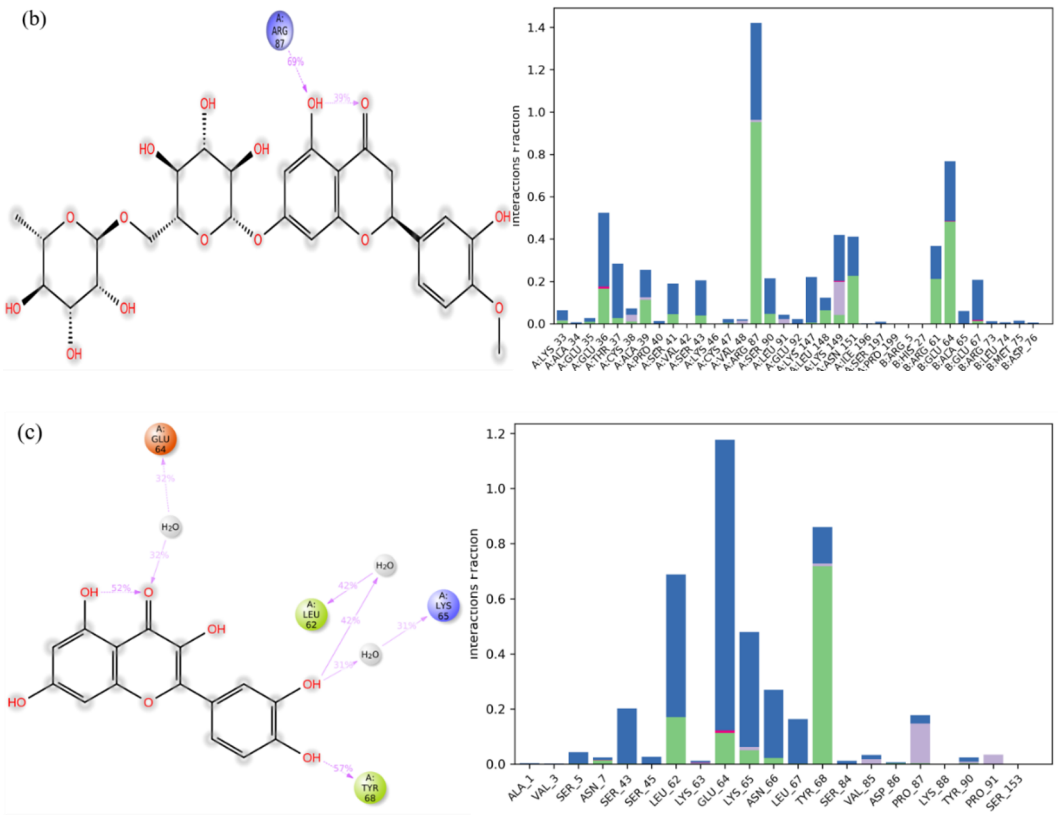

Figure 8. Illustrative diagram depicting the various interactions between the protein-ligand complexes derived from the respective 100 ns simulations: (a) MEK1-Ellagic acid (b) CDK4-Hesperidin (c) IL1-Quercetin. Hydrophobic contacts (blue bars) and hydrogen bonds (green bars).

(a)

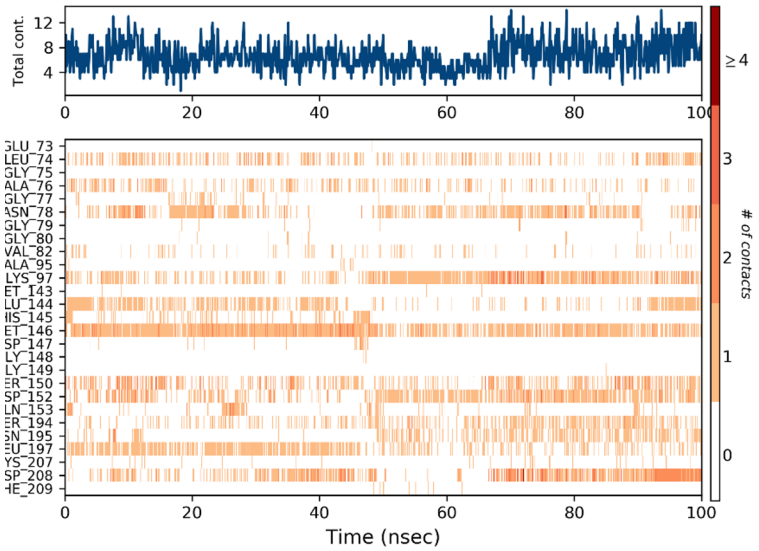

(b)

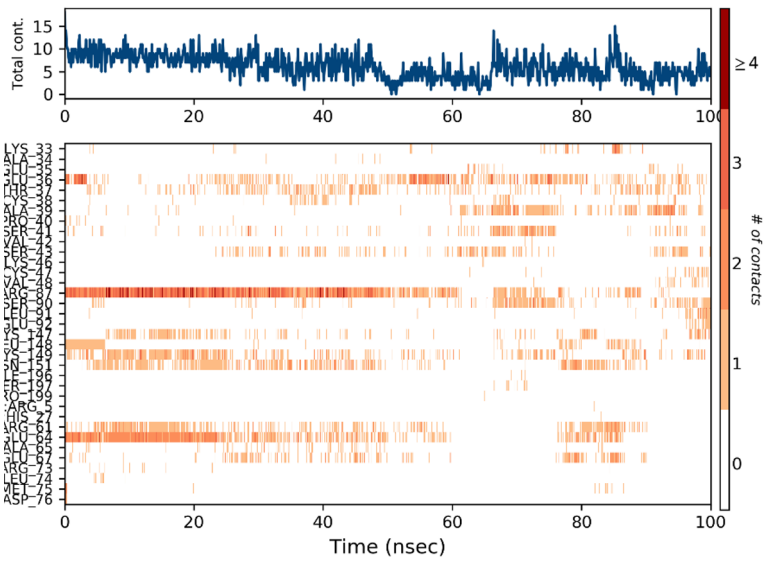

(c)

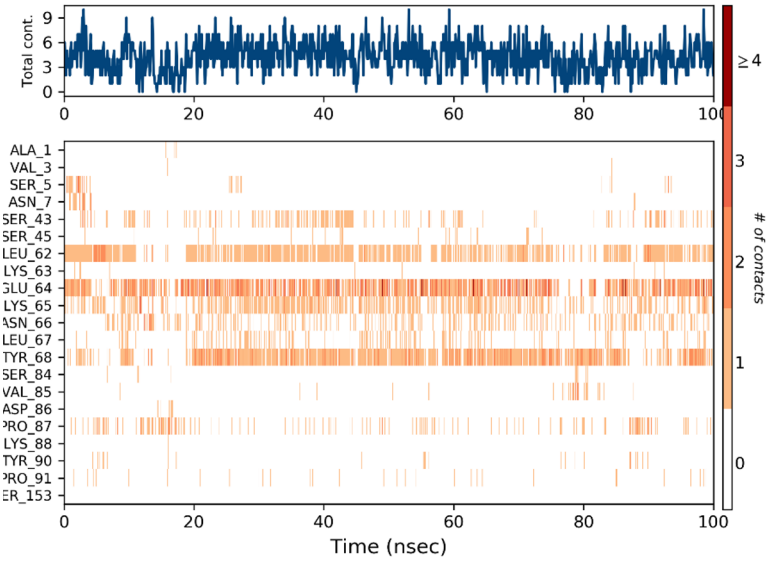

Figure 9. Contact map and timeline of interactions among amino acid residues of the complexes over 100 ns in molecular dynamics simulation: (a) MEK1-Ellagic acid, (b) CDK4-Hesperidin, (c) IL1-Quercetin

3.4 MM-GBSA calculations

The binding free energy of each complex from 0 ns to 100 ns was calculated using this method. The total binding energy ΔGbind depends on non-bonded interactions, including Lipophilic (Gbind Lipo), van der Waals (Gbind vdW), Coulombic (Gbind Coulomb), and Hydrogen Bonding (Gbind H bond) (Table 6).

The binding free energies (ΔG_bind) for the MEK1-Ellagic acid, CDK4-Hesperidin, and IL1-Quercetin complexes were calculated to be -64.33 ± 14.38, -56.74 ± 19.20, and -35.01 ± 6.30 kcal/mol, respectively. These values suggest that Ellagic acid has the strongest binding affinity to MEK1, followed by Hesperidin to CDK4, and Quercetin to IL1. Analysing the energy components further reveals that van der Waals interactions (vdW) contribute the most significantly to binding for all complexes, with contributions of -41.24 ± 1.49 kcal/mol for MEK1-Ellagic acid, -36.27 ± 14.15 kcal/mol for CDK4-Hesperidin, and -25.93 ± 6.32 kcal/mol for IL1-Quercetin. Lipo contributions also play a substantial role in all interactions, with values of -23.40 ± 2.71, -24.98 ± 2.39, and -12.62 ± 0.66 kcal/mol, respectively. In terms of Coulombic interactions, CDK4-Hesperidin (-30.34 ± 5.50 kcal/mol) shows a stronger electrostatic component compared to the other complexes, followed by MEK1-Ellagic acid (-23.81 ± 10.34kcal/mol) and IL1-Quercetin (-19.19 ± 6.79).

In terms of hydrogen bonding, CDK4-Hesperidin shows the highest (-3.68 ± 4.16 kcal/mol), while MEK1-Ellagic acid and IL1-Quercetin show -1.60 ± 0.49 and -1.17± 0.83 kcal/mol, respectively. Notably, packing energy only contributes slightly to MEK1-Ellagic acid binding (-1.26 kcal/mol), and was found to be negligible for the other two complexes, as the interactions in both the complexes are driven by van der Waals and lipophilic interactions rather than tight steric packing within the binding pocket. Overall, the MM-GBSA calculations derived from MD simulations validated the binding energies obtained from molecular docking, reinforcing the robustness of the computational predictions

Table 6. Average MM-GBSA binding energy calculations of the complexes after 100 ns from MD simulation trajectories.

Energies (Kcal/mol)	MEK1-Ellagic acid	CDK4-Hesperidin	IL1- Quercetin
dG_{bind}	-64.33 ± 14.38	-56.74 ± 19.20	-35.01 ± 6.30
dG_{bind} Lipo	-23.40 ± 2.71	-24.98 ± 2.39	-12.62 ± 0.66
dG_{bind} vdW	-41.24 ± 1.49	-36.27 ± 14.15	-25.93 ± 6.32
dG_{bind} Coulomb	-23.81 ± 10.34	-30.34 ± 5.50	-19.19 ± 6.79
dG_{bind} H_{bond}	-1.60 ± 0.49	-3.68 ± 4.16	-1.17± 0.83

4. Discussion

According to WHO statistics, skin cancer is among the most frequently diagnosed cancers worldwide, particularly among individuals with lighter skin tones (Samarasinghe et al., 2012). As a result, developing effective treatment strategies for skin cancer has become a critical issue. While many treatment options are available, they are often expensive and associated with significant side effects. Consequently, there is a growing interest in medical plants and their bioactive compounds, which have been utilized for centuries to address various ailments, including skin cancer. Several studies have shown that phytocompounds often have fewer side effects and exhibit non-toxic antioxidant, anticancer, and antitumor activities (Choudhari et al., 2020). Using computational methods, it has now become quicker to explore the molecular mechanism of these phytocompounds.

A molecular docking study was conducted on 15 compounds from the peel of *C. limetta* against selected molecular targets (MEK1, CDK4, and IL1) involved in cell proliferation and apoptosis and their binding patterns were analyzed. The current study showed that out of 15 selected compounds, Ellagic acid exhibited a good docking score (–10.5 kcal/mol) against MEK1 without violating any of the parameters of Lipinski's Rule of Five (LR05). Additionally, despite breaking three of Lipinski's rules, Hesperidin (−8.8 kcal/mol) demonstrated a higher docking score against CDK4. However, Quercetin (−7.6 kcal/mol) exhibited the highest binding energy to IL1 without deviating from any of the LR05 characteristics.

Other phytocompounds, including Ascorbic Acid, Caryophyllene, D-Limonene, Oleic Acid, Apigenin, Gallic Acid, Procyanidin, Caffeic Acid, Ferulic Acid, and Naringenin, also showed potential scores against MEK1, CDK4, and IL1 without violating any of the parameters of LR05, whereas Gallagic acid and Rutin violated a few rules. However, their pharmacokinetic and toxicity prediction must be considered when evaluating their therapeutic potential. Notably, caffeic acid, though it exhibited favorable binding affinity, toxicity prediction analysis suggested potential safety concerns, including possible carcinogenicity, which limits its applicability as a drug candidate

The selection of MEK1, CDK4, and IL1 as targets for cancer therapy is supported by existing literature. Similar to our study, AlZahrani et al. (2022) reported binding affinities, ranging from −10.4 kcal/mol to −10.8 kcal/mol for various flavonoids against MEK1, suggesting flavonoids as a promising source of targeted anticancer therapy. Furthermore, Shi et al. (2021) stated that targeting the dysregulation of the CDK4 pathway is effective for the treatment of mucosal

melanoma; therefore, we focused on targeting CDK4 for skin cancer management. The relevance of IL-1 targeting is further supported by Bou-Dargham et al. (2017), who described IL-1 agonists as crucial mediators in various benign and malignant skin conditions and proposed as a primary target for immunotherapy in skin cancer.

Previous studies also emphasize the anticancer potential of the selected phytocompounds. Ellagic acid has been reported to inhibit PI3K in endometrial cancer (Wang et al., 2019). Similarly, quercetin has been shown to induce apoptosis in murine melanoma cells by inhibiting PI3K activity (Zhang et al., 2005). Furthermore, hesperidin has shown anticancer efficacy against murine melanoma B16BL6 cells and induces apoptosis and inhibition of metastasis in C57BL/6 mice (Byun et al., 2019).

Substantial experimental evidence further supports the therapeutic potential of plant-derived peel extracts and their compounds in melanoma models. Bashir et al. (2022) conducted an *in vivo* test using a mouse model of DMBA-induced skin cancer and demonstrated that the topical administration of a mixture of coumarin and quercetin reduced the viability of melanoma cells and induced apoptosis.

Additionally, previous studies on *Punica granatum* peel extracts have demonstrated significant anticancer activity against B16-F10 and HTB140 melanoma cell lines by activating PPARs signaling, resulting in the downregulation of gene expression (VEGF, Ki-67, and CD31) implicated in melanoma progression (Seifabadi et al. 2019; Keta et al., 2020). Similarly, the anticancer effect of banana peels was investigated in both *in vitro* and *in vivo* models, MCF and HeLa cells (Haasan et al., 2021). Supporting the evidence of *C. limetta* waste material, Rasool et al. (2021) and Shyam (2019) reported the antioxidant properties of the ethanolic and methanolic extract of *C. limetta* peel and its cytotoxic effects on Hep G2 and MCF-7 cell lines, highlighting the extract's potential as a source of bioactive anticancer compounds.
ADMET properties are crucial for drug development, influencing molecular weight, drug-likeness, and solubility, which affect absorption and delivery to target sites. Importantly, selected candidates must be non-toxic to the host. Our ADMET analysis indicated that ellagic acid, hesperidin, and quercetin exhibit favorable pharmacological profiles. However, due to its hydrophilic nature, hesperidin's low permeability may hinder its bioavailability during membrane absorption. It is important to note that the therapeutic profiles described here are of oral administration, but the bioavailability of the drug is also influenced by the formulation and the administration route. Maulydia et al. (2022) suggested that hesperidin could serve as a viable drug candidate despite not meeting LR05 criteria.

Overall, the present findings suggest that selected phytocompounds, particularly ellagic acid, quercetin, and hesperidin, exhibit significant potential as a lead molecule for targeted skin cancer management. However, it is necessary to conduct *in vitro* and *in vivo* studies, along with clinical trials, to further validate the anticancer effects

5. Conclusion

The outcome of this study reveals the anti-cancer potential of *Citrus limetta* peel extracts through computational analysis. The molecular docking analysis revealed that the three protein-ligand complexes — Ellagic acid-MEK1 (–10.5 kcal/mol), Hesperidin-CDK4 (–8.8 kcal/mol), and Quercetin-IL1 (−7.6 kcal/mol) — exhibited the highest binding affinities among the screened compounds.

Molecular dynamics simulation further confirmed the structural stability of the ellagic acid-MEK1 and quercetin-IL1 complexes throughout the 100 ns simulation. However, Hesperidin-CDK4 showed conformational changes, possibly due to the large molecular size of hesperidin; this may be clarified through simulations extending beyond 100 ns.

ADMET prediction further demonstrated that the selected compounds exhibit nontoxic profiles and have pharmacological properties, supporting their drug-likeliness properties. Collectively these findings highlight the potential of *Citrus limetta* peel extracts and suggest that ellagic acid, quercetin, and hesperidin can be used as target drug candidates and thus can be further analyzed as lead molecules for the drug development against skin cancer. However, *in vitro*, *in vivo*, and clinical trials for their efficacy, effectiveness, and safety must be validated further.

References

1. AlZahrani, W. M., AlGhamdi, S. A., Zughaibi, T. A., & Rehan, M. (2022). Exploring the natural compounds in flavonoids for their potential inhibition of cancer therapeutic target MEK1 using computational methods. Pharmaceuticals, 15(2), 195.
2. Bahar, M. E., Kim, H. J., & Kim, D. R. (2023). Targeting the RAS/RAF/MAPK pathway for cancer therapy: from mechanism to clinical studies. Signal transduction and targeted therapy, 8(1), 455.
3. Banerjee, P., Eckert, A. O., Schrey, A. K., & Preissner, R. (2018). ProTox-II: a webserver for the prediction of toxicity of chemicals. Nucleic acids research, 46(W1), W257-W263.
4. Bashir, A., Asif, M., Saadullah, M., Saleem, M., Khalid, S. H., Hussain, L., ... & Chohan, T. A. (2022). Therapeutic potential of standardized extract of melilotus indicus (L.) all. and its phytochemicals against skin cancer in animal model: in vitro, in vivo, and in silico studies. ACS omega, 7(29), 25772-25782.
5. Bou-Dargham, M. J., Khamis, Z. I., Cognetta, A. B., & Sang, Q. X. A. (2017). The role of interleukin-1 in inflammatory and malignant human skin diseases and the rationale for targeting interleukin-1 alpha. Medicinal research reviews, 37(1), 180-216.
6. Bowers, K. J., Chow, D. E., Xu, H., Dror, R. O., Eastwood, M. P., Gregersen, B. A., Klepeis, J. L., Kolossvary, I., Moraes, M. A., Sacerdoti, F. D., & Shaw, D. E. (2006). Scalable algorithms for molecular dynamics simulations on commodity clusters. In Proceedings of the 2006 ACM/IEEE Conference on Supercomputing (p. 43).
7. Buyukkurt, O. K., Guclu, G., Kelebek, H., & Selli, S. (2019). Characterization of phenolic compounds in sweet lime (Citrus limetta) peel and freshly squeezed juices by LC-DAD ESI-MS/MS and their antioxidant activity. Journal of Food Measurement and Characterization, 13, 3242-3249.
8. Byun, E.B., Kim, H.M., Song, H.Y. and Kim, W.S., 2019. Hesperidin structurally modified by gamma irradiation induces apoptosis in murine melanoma B16BL6 cells and inhibits both subcutaneous tumor growth and metastasis in C57BL/6 mice. Food Chem. Toxicol. 127, 19-30.
9. Chauhan, P. (2018). Skin cancer and role of herbal medicines. Asian Journal of Pharmacy and Pharmacology, 4(4), 404-412.
10. Cheng, Y., & Tian, H. (2017). Current development status of MEK inhibitors. Molecules, 22(10), 1551-1571.
11. Chinembiri, T. N., Du Plessis, L. H., Gerber, M., Hamman, J. H., & Du Plessis, J. (2014). Review of natural compounds for potential Skin Cancer treatment. Molecules, 19(8), 11679-11721.
12. Choudhari, A. S., Mandave, P. C., Deshpande, M., Ranjekar, P., & Prakash, O. (2020). Phytochemicals in cancer treatment: From preclinical studies to clinical practice. Frontiers in pharmacology, 10, 1614.
13. Garlanda, C., & Mantovani, A. (2021). Interleukin-1 in tumor progression, therapy, and prevention. Cancer cell, 39(8), 1023-1027.
14. Garutti, M., Targato, G., Buriolla, S., Palmero, L., Minisini, A. M., & Puglisi, F. (2021). CDK4/6 inhibitors in melanoma: a comprehensive review. Cells, 10(6), 1334-1350.
15. Grimaldi, A. M., Simeone, E., Festino, L., Vanella, V., Strudel, M., & Ascierto, P. A. (2017). MEK inhibitors in the treatment of metastatic melanoma and solid tumors. American journal of clinical dermatology, 18(6), 745-754.
16. Guo, L., Qi, J., Wang, H., Jiang, X., & Liu, Y. (2020). Getting under the skin: The role of CDK4/6 in melanomas. European Journal of Medicinal Chemistry, 204, 112531.
17. Hamilton, E., & Infante, J. R. (2016). Targeting CDK4/6 in patients with cancer. Cancer treatment reviews, 45, 129-138.
18. Hassan, M. H. (2021). In vitro and in vivo Study of Banana Peel Extract Anti Toxicity. Medico-legal Update, 21(2).
19. Kaloni, D., Chakraborty, D., Tiwari, A., & Biswas, S. (2020). In silico studies on the phytochemical components of Murraya koenigii targeting TNF-α in rheumatoid arthritis. Journal of Herbal Medicine, 24, 100396.
20. Kandeel, M., Iqbal, M. N., Ali, I., Malik, S., Malik, A., & Sehgal, S. A. (2023). Comprehensive in silico analyses of flavonoids elucidating the drug properties against kidney disease by targeting AIM2. Plos one, 18(5), e0285965.
21. Keta, O. D., Deljanin, M., Petković, V., Zdunić, G., Janković, T., Živković, J., ... & Šavikin, K. (2020). Pomegranate (Punica granatum L.) Peel Extract: potential cytotoxic agent against different cancer cell lines. Records of Natural Products, 14(5), 326-339.
22. Khan, A. A., Mahmood, T., Siddiqui, H. H., & Akhtar, J. (2016). Phytochemical and pharmacological properties on C. limetta (Mosambi). Journal of Chemical and Pharmaceutical Research, 8(3), 555-563.
23. Lolok, N., Sumiwi, S. A., Muhtadi, A., Susilawati, Y., Hendriani, R., Ramadhan, D. S. F., ... & Sahidin, I. (2022). Molecular docking and molecular dynamics studies of bioactive compounds contained in noni fruit (Morinda citrifolia L.) against human pancreatic α-amylase. Journal of Biomolecular Structure and Dynamics, 40(15), 7091-7098.
24. Malcova, H., Strizova, Z., Milota, T., Striz, I., Sediva, A., Cebecauerova, D. et al. (2021). IL-1 inhibitors in the treatment of monogenic periodic fever syndromes: from the past to the future perspectives. Frontiers in Immunology, 11, 619257.

25. Maulydia, N. B., Tallei, T. E., Ginting, B., Idroes, R., & Faradilla, M. (2022). Analysis of flavonoid compounds of Orange (Citrus sp.) peel as anti-main protease of SARS-CoV-2: A molecular docking study. IOP Conference Series: Earth and Environmental Science, 951(1), 012078.
26. Maurya, A. K., Mohanty, S., Pal, A., Chanotiya, C. S., & Bawankule, D. U. (2018). The essential oil from C. limetta Risso peels alleviates skin inflammation: In-vitro and in-vivo study. Journal of ethnopharmacology, 212, 86-94.
27. Mendie, L. E., & Hemalatha, S. (2022). Molecular docking of phytochemicals targeting GFRs as therapeutic sites for cancer: an in silico study. Applied biochemistry and biotechnology, 194(1), 215-231.
28. Noor, H., Ikram, A., Rathinavel, T., Kumarasamy, S., Nasir Iqbal, M., & Bashir, Z. (2022). Immunomodulatory and anti-cytokine therapeutic potential of curcumin and its derivatives for treating COVID-19 – a computational modeling. Journal of Biomolecular Structure and Dynamics, 40(13), 5769-5784.
29. Qi, J., & Ouyang, Z. (2022). Targeting CDK4/6 for anticancer therapy. Biomedicines, 10(3), 685.
30. Rasool, S., Ahmed, H., Uttra, M. M., Uttra, A. M., Khan, M. R., Zakir, K. A., ... & Saleem, F. (2021). Antioxidant and anti-cancer effect of ethanolic extract of citrus fruits on Hep G2 and MCF-7 cell lines. Journal of Pharmaceutical Research International, 33(49A), 84-90.
31. Rolta, R., Yadav, R., Salaria, D., Trivedi, S., Imran, M., Sourirajan, A., ... & Dev, K. (2021). In silico screening of hundred phytocompounds of ten medicinal plants as potential inhibitors of nucleocapsid phosphoprotein of COVID-19. Journal of Biomolecular Structure and Dynamics, 39(18), 7017-7034.
32. Sakshi, C., Harikrishnan, A., Jayaraman, S., Choudhury, A. R., & Veena, V. (2022). Predictive medicinal metabolites from Momordica dioica against comorbidity related proteins of SARS-CoV-2 infections. Journal of Biomolecular Structure and Dynamics, 40(11), 5175-5188.
33. Samarasinghe, V., & Madan, V. (2012). Nonmelanoma Skin Cancer. Journal of Cutaneous and Aesthetic Surgery, 5(1), 3-10.
34. Seifabadi, S., Vaseghi, G., Ghannadian, M., & Javanmard, S. H. (2019). Standardized Punica Granatum pericarp extract, suppresses tumor proliferation and angiogenesis in a mouse model of melanoma: possible involvement of PPARα and PPARγ pathways. Iranian journal of pharmaceutical research: IJPR, 18(1), 348.
35. Sever, R., & Brugge, J. S. (2015). Signal transduction in cancer. Cold Spring Harbor perspectives in medicine, 5(4), a006098.
36. Shi, C. J., Xu, S. M., Han, Y., Zhou, R., & Zhang, Z. Y. (2021). Targeting cyclin-dependent kinase 4/6 as a therapeutic approach for mucosal melanoma. Melanoma Research, 31(6).
37. Shyam, J. (2019). The Phytochemical and Pharmacological Activity of C. limetta Peel Extracts. Journal of Global Biosciences, 8(8), 6382-6396.
38. Thirumalaisamy, R., Aroulmoji, V., Iqbal, M. N., Saride, S., Bhuvaneswari, M., Deepa, M., ... & Khan, R. (2023). Molecular insights of hyaluronic acid–ethambutol and hyaluronic acid–isoniazid drug conjugates act as promising novel drugs for the treatment of tuberculosis. Journal of Biomolecular Structure and Dynamics, 41(8), 3562-3573.
39. Unsworth, A. J., Bye, A. P., Kriek, N., Sage, T., Osborne, A. A. et al. (2019). Cobimetinib and trametinib inhibit platelet MEK but do not cause platelet dysfunction. Platelets, 30(6), 762-772.
40. Wander, S. A., O'Brien, N., Litchfield, L. M., O'Dea, D., Morato Guimaraes, C. et al. (2022). Targeting CDK4 and 6 in cancer therapy: emerging preclinical insights related to abemaciclib. The oncologist, 27(10), 811-821.
41. Wang, F., Chen, J., Xiang, D., Lian, X., Wu, C., & Quan, J. (2020). Ellagic acid inhibits cell proliferation, migration, and invasion in melanoma via EGFR pathway. American Journal of Translational Research, 12(5), 2295.
42. Yousuf, M., Khan, P., Shamsi, A., Shahbaaz, M., Hasan, G. M., et al. (2020). Inhibiting CDK6 activity by quercetin is an attractive strategy for cancer therapy. ACS omega, 5(42), 27480-27491.
43. Zhang, X.M., Chen, J., Xia, Y.G. and Xu, Q. (2005). Apoptosis of murine melanoma B16-BL6 cells induced by quercetin targeting mitochondria, inhibiting expression of PKC-α and translocating PKC-δ. Cancer Chemotherapy and Pharmacology. 55(3), 251-262.